The Journal of Chemical Physics

RESEARCH ARTICLE | FEBRUARY 25 2025

Application of the noncollinear Scalmani–Frisch formalism to current density functional theory

Yannick J. Franzke ; Ansgar Pausch ; Christof Holzer

J. Chem. Phys. 162, 084104 (2025)
https://doi.org/10.1063/5.0246433

The Journal of Chemical Physics ARTICLE pubs.aip.org/aip/jcp

Application of the noncollinear Scalmani–Frisch formalism to current density functional theory

Cite as: J. Chem. Phys. 162, 084104 (2025); doi: 10.1063/5.0246433
Submitted: 1 November 2024 • Accepted: 4 February 2025 •
Published Online: 25 February 2025

Yannick J. Franzke,[1,2,a)] Ansgar Pausch,[3,a)] and Christof Holzer[4,a)]

AFFILIATIONS

[1] Otto Schott Institute of Materials Research, Friedrich Schiller University Jena, Löbdergraben 32, 07743 Jena, Germany
[2] Institute of Nanotechnology, Karlsruhe Institute of Technology (KIT), Kaiserstraße 12, 76131 Karlsruhe, Germany
[3] Theoretical Chemistry, Vrije Universiteit Amsterdam, 1081HV Amsterdam, The Netherlands
[4] Institute of Theoretical Solid State Physics, Karlsruhe Institute of Technology (KIT), Kaiserstraße 12, 76131 Karlsruhe, Germany

[a)] **Authors to whom correspondence should be addressed:** yannick.franzke@kit.edu; a.i.pausch@vu.nl; and holzer@kit.edu

ABSTRACT

We generalize the noncollinear formalism proposed by Scalmani and Frisch [J. Chem. Theory Comput. **8**, 2193 (2012)] to include the particle and spin current densities for *meta*-generalized gradient approximations and local hybrid functionals. This allows us to fully include the impact of spin–orbit coupling in relativistic calculations and for applications to finite magnetic fields. For the latter, we use London atomic orbitals to ensure gauge origin invariance. It is shown that this formalism is superior to the more common canonical noncollinear approach in relativistic calculations, as it naturally includes all three spin current densities in the closed-shell limit and avoids the projection onto the spin magnetization vector. This is important to easily restore rotational invariance in this limit. In addition, the Scalmani–Frisch approach can be made numerically stable and may lead to a nonvanishing local magnetic torque. However, both formalisms are rotationally invariant for open-shell systems and in finite magnetic fields.

I. INTRODUCTION

Many sources can induce non-vanishing paramagnetic current densities within molecules and materials, including external magnetic fields or relativistic effects such as spin–orbit coupling (SOC). Consequently, the exchange-correlation functional in density functional theory (DFT) should not only depend on density variables but also on the paramagnetic current density.[1] In the framework of Kohn–Sham current density functional theory (CDFT), these currents are explicitly taken into account. Here, density functional approximations (DFAs) depending on the kinetic energy density, such as *meta*-generalized gradient approximations (*meta*-GGAs) and most local hybrid functionals (LHFs), can be generalized to naturally include the paramagnetic current density.[2,3] This holds for both closed-shell and open-shell systems and can be of great importance in practical calculations. For instance, the standard kinetic energy density becomes gauge variant, and this leads to a loss of rotational and translational invariance in finite magnetic fields. Therefore, the CDFT framework must be applied in strong magnetic fields.[4–18] Similar findings also hold for electromagnetic response calculations, where the current densities need to be included in the exchange-correlation kernel but not in the ground-state potential.[19–30] Recently, CDFT was also applied to two-component spin–orbit calculations.[31–35] For instance, a detailed study for many properties and functionals was carried out by the present authors in Ref. 31 and showed that the current densities have a pronounced impact on the Minnesota functionals,[36,37] r^{2}SCAN,[38,39] and TASK.[40] Other approximations such as the Tao–Mo functional[41] or TPSS[42] and TPSSh[43] are rather insensitive toward the inclusion of the current density.

So far, the canonical noncollinear formalism,[44–50] which relies on a projection of the spin densities, gradient of the spin densities, spin kinetic energy density, and paramagnetic spin current density variables onto the spin magnetization, was applied for open-shell systems. Scalmani and Frisch (SF) proposed an alternative formalism avoiding this projection.[51] Their ansatz leads to a non-vanishing local torque on the magnetization,[52–54] yet the zero-torque theorem[55] is preserved.[52] Unfortunately, the SF ansatz is currently

only available for GGAs and *meta*-GGAs in DFT, but not CDFT. Therefore, we extend the SF approach to CDFT and local hybrids. This subsequently allows us to study its impact on various properties in the present work.

II. THEORY

A. Canonical noncollinear formalism

We start by briefly reviewing the canonical (can) formalism[44–50] for spin–orbit current density functional theory[31,32] and magnetic fields.[17,18] Special attention is paid to the construction of the spin-up and spin-down quantities. The electron density and spin magnetization are defined as

$$\rho^0 = \sum_j \varphi_j^\dagger \varphi_j, \tag{1}$$

$$m_u = \sum_j \varphi_j^\dagger \sigma_u \varphi_j, \tag{2}$$

with σ_u being the traceless Pauli spin matrices, and j refers to the Kohn–Sham spinors φ_j. The noncollinear spin magnetization density follows as

$$m^s = \sqrt{m_x^2 + m_y^2 + m_z^2}, \tag{3}$$

and the spin-up and spin-down densities are

$$\rho^{\uparrow,\downarrow} = (\rho^0 \pm m^s)/2. \tag{4}$$

For GGAs, the generalized gradient variables are

$$\gamma^{\sigma\sigma'} = \frac{1}{4}(\vec{\nabla}\rho^\sigma)\cdot(\vec{\nabla}\rho^{\sigma'}) \quad \text{with } \sigma,\sigma' \in \{\uparrow,\downarrow\}, \tag{5}$$

and

$$\vec{\nabla}\rho^{\uparrow,\downarrow} = \frac{1}{2}\left(\vec{\nabla}\rho^0 \pm \frac{1}{m^s}\left[m_x\vec{\nabla}m_x + m_y\vec{\nabla}m_y + m_z\vec{\nabla}m_z\right]\right). \tag{6}$$

For *meta*-GGAs, the particle and spin kinetic energy density are further defined as

$$\tau^0 = \frac{1}{2}\sum_j \sum_\alpha (\hat{p}_\alpha\varphi_j)^\dagger(\hat{p}_\alpha\varphi_j), \tag{7}$$

$$u_u = \frac{1}{2}\sum_j \sum_\alpha (\hat{p}_\alpha\varphi_j)^\dagger\sigma_u(\hat{p}_\alpha\varphi_j), \tag{8}$$

with the momentum operator $\hat{\vec{p}} = -i\vec{\nabla}$. α refers to the spatial Cartesian directions and u to the spin. Projection of the spin kinetic energy density onto the spin magnetization vector

$$u^s = \frac{1}{m^s}\left[m_x u_x + m_y u_y + m_z u_z\right], \tag{9}$$

again leads to the spin-up and spin-down kinetic energy densities

$$\tau^{\uparrow,\downarrow} = (\tau^0 \pm u^s)/2. \tag{10}$$

To ensure gauge invariance, the current densities need to be considered. Here, the paramagnetic current density reads

$$j_\alpha^0 = -\frac{i}{2}\sum_j \left[\varphi_j^\dagger(\nabla_\alpha\varphi_j) - (\nabla_\alpha\varphi_j)^\dagger\varphi_j\right], \tag{11}$$

and the corresponding spin current densities are

$$Y_{\alpha,u} = -\frac{i}{2}\sum_j \left[\varphi_j^\dagger\sigma_u(\nabla_\alpha\varphi_j) - (\nabla_\alpha\varphi_j)^\dagger\sigma_u\varphi_j\right]. \tag{12}$$

We note that this spin-current density must not be confused with the spin-current density $-\frac{1}{2}(\vec{\nabla}\times\vec{\rho})$ used in quantum theory. To construct the spin-up and down quantities, we project the spin current density on the spin magnetization

$$Y_\alpha^s = \frac{1}{m^s}\left[m_x Y_{\alpha,x} + m_y Y_{\alpha,y} + m_z Y_{\alpha,z}\right], \tag{13}$$

leading to

$$j_\alpha^{\uparrow,\downarrow} = (j_\alpha^0 \pm Y_\alpha^s)/2. \tag{14}$$

Finally, the gauge invariant generalized kinetic energy densities are given by

$$\tilde{\tau}^{\uparrow,\downarrow} = \tau^{\uparrow,\downarrow} - \frac{1}{2}\frac{|\vec{j}^{\uparrow,\downarrow}|^2}{\rho^{\uparrow,\downarrow}}. \tag{15}$$

The remaining working equations for the exchange-correlation potential are given in Refs. 31 and 32 for finite and periodic systems, respectively. Note that m_u and j_α^0 vanish for closed-shell systems, while ρ^0 and $Y_{\alpha,u}$ are generally non-zero. In this regard, a crucial shortcoming of this formalism is that the spin current densities are projected onto the spin magnetization.

B. Scalmani–Frisch noncollinear formalism

Another formalism was outlined by Scalmani, Frisch, and coworkers.[51–53] This ansatz avoids the detrimental projection onto the spin magnetization vector and may also lead to a nonvanishing local magnetic torque. The spin-up and spin-down electron density is defined as in the canonical formalism. However, the gradient variables read

$$\gamma_{\uparrow\uparrow,\downarrow\downarrow} = \frac{1}{4}\left[\vec{\nabla}\rho^0\cdot\vec{\nabla}\rho^0 + \vec{\nabla}\mathbf{m}\odot\vec{\nabla}\mathbf{m}\right] \pm \frac{f_\nabla}{2}\Gamma, \tag{16}$$

$$\Gamma = \sqrt{\left(\vec{\nabla}\rho^0\cdot\vec{\nabla}\mathbf{m}\right)\circ\left(\vec{\nabla}\rho^0\cdot\vec{\nabla}\mathbf{m}\right)}, \tag{17}$$

$$\gamma_{\uparrow\downarrow} = \frac{1}{4}\left[\vec{\nabla}\rho^0\cdot\vec{\nabla}\rho^0 - \vec{\nabla}\mathbf{m}\odot\vec{\nabla}\mathbf{m}\right], \tag{18}$$

$$f_\nabla = \mathrm{sgn}\left(\left[\vec{\nabla}\rho^0\cdot\vec{\nabla}\mathbf{m}\right]\circ\mathbf{m}\right), \tag{19}$$

where $\cdot$ refers to the scalar coordinates, $\circ$ refers to the spin coordinates, and $\odot$ refers to a scalar product in both spaces. Vectors in

spatial space use an arrow, whereas bold letters are used for vectors in spin space. The kinetic energy densities are defined as

$$\tau_{\uparrow,\downarrow} = \frac{1}{2}\left(\tau^0 \pm f_\tau \sqrt{\mathbf{u} \circ \mathbf{u}}\right), \tag{20}$$

$$f_\tau = \mathrm{sgn}\left(\mathbf{u} \circ \mathbf{m}\right). \tag{21}$$

Note that the alternative expressions of Ref. 53 are used in regions with (almost) vanishing spin magnetization (m^s below 10^{-16} herein for *meta*-GGAs) within this work to increase the numerical stability. This was deemed to be important for second derivatives within the exchange-correlation kernel. Other stabilization procedures were also suggested in Ref. 56.

Here, we propose to generalize the current densities accordingly

$$j_\alpha^{\uparrow,\downarrow} = \frac{1}{2}\left(j_\alpha^0 \pm f_{j,\alpha} \sqrt{\mathbf{Y}_\alpha \circ \mathbf{Y}_\alpha}\right), \tag{22}$$

$$f_{j,\alpha} = \mathrm{sgn}\left(\mathbf{Y}_\alpha \circ \mathbf{m}\right). \tag{23}$$

For clarity, note that $\mathbf{Y}_\alpha$ is a vector in spin space for the spatial component α. The generalized kinetic energy density is again constructed with the individual spin-up and down quantities as in Eq. (15), which reduces to

$$\tilde{\tau}^{\uparrow,\downarrow} = \tau^{\uparrow,\downarrow} - \frac{1}{8}\frac{\vec{\mathbf{Y}} \odot \vec{\mathbf{Y}}}{\rho^{\uparrow,\downarrow}}, \tag{24}$$

in the closed-shell or (time-reversal-symmetric) Kramers-restricted limit. Here, the up and down quantities of the density and the (generalized) kinetic energy density are identical, i.e., $\rho^{\uparrow,\downarrow} = \frac{1}{2}\rho^0$ and $\tau^{\uparrow,\downarrow} = \frac{1}{2}\tau^0$. Hence, the total generalized kinetic energy density follows as the sum of both quantities,

$$\tilde{\tau}^0 = \tau^0 - \frac{1}{2}\frac{\vec{\mathbf{Y}} \odot \vec{\mathbf{Y}}}{\rho^0}. \tag{25}$$

Therefore, the same generalized kinetic energy density as in Ref. 34, which is restricted to the closed-shell limit, is obtained.

For open-shell systems, the exchange-correlation potential consists of a total or particle and a spin contribution. Following the derivation in Ref. 31, the so-called total part of the exchange-correlation potential becomes

$$\begin{aligned} X^0_{\mu\nu} = {} & \frac{1}{2}\int\left[\frac{\partial g^{\mathrm{XC}}}{\partial \rho^\uparrow} + \frac{\partial g^{\mathrm{XC}}}{\partial \rho^\downarrow}\right]\mu\ \nu\ \mathrm{d}^3r + \frac{1}{2}\int\left[\frac{|\vec{j}^\uparrow|^2}{2\left(\rho^\uparrow\right)^2}\frac{\partial g^{\mathrm{XC}}}{\partial \tilde{\tau}^\uparrow} + \frac{|\vec{j}^\downarrow|^2}{2\left(\rho^\downarrow\right)^2}\frac{\partial g^{\mathrm{XC}}}{\partial \tilde{\tau}^\downarrow}\right]\mu\ \nu\ \mathrm{d}^3r - \frac{1}{2}\int\left[\frac{\partial g^{\mathrm{XC}}}{\partial \gamma^{\uparrow\uparrow}} + \frac{\partial g^{\mathrm{XC}}}{\partial \gamma^{\downarrow\downarrow}} + \frac{\partial g^{\mathrm{XC}}}{\partial \gamma^{\uparrow\downarrow}}\right]\vec{\nabla}\rho^0 \\ & \cdot\left[\{\vec{\nabla}\mu\}\nu + \mu\{\vec{\nabla}\nu\}\right]\mathrm{d}^3r - \frac{1}{2}\int\left[\frac{\partial g^{\mathrm{XC}}}{\partial \gamma^{\uparrow\uparrow}} - \frac{\partial g^{\mathrm{XC}}}{\partial \gamma^{\downarrow\downarrow}}\right]f_\nabla\frac{\left(\vec{\nabla}\rho^0 \cdot \vec{\nabla}\mathbf{m}\right) \circ \vec{\nabla}\mathbf{m}}{\Gamma}\ \cdot\left[\{\vec{\nabla}\mu\}\nu + \mu\{\vec{\nabla}\nu\}\right]\mathrm{d}^3r \\ & + \frac{1}{4}\int\left[\frac{\partial g^{\mathrm{XC}}}{\partial \tilde{\tau}_\uparrow} + \frac{\partial g^{\mathrm{XC}}}{\partial \tilde{\tau}_\downarrow}\right]\left[\vec{\nabla}\mu\right]\cdot\left[\vec{\nabla}\nu\right]\mathrm{d}^3r + \frac{\mathrm{i}}{4}\int\sum_\alpha\left[\frac{j_\alpha^\uparrow}{\rho^\uparrow}\frac{\partial g^{\mathrm{XC}}}{\partial \tilde{\tau}^\uparrow} + \frac{j_\alpha^\downarrow}{\rho^\downarrow}\frac{\partial g^{\mathrm{XC}}}{\partial \tilde{\tau}^\downarrow}\right]\left[\{\nabla_\alpha\mu\}\nu - \mu\{\nabla_\alpha\nu\}\right]\mathrm{d}^3r, \end{aligned} \tag{26}$$

where μ and ν denote the spatial basis functions and g^{XC} describes the density functional approximation. Here, were assumed $\frac{\partial g^{\mathrm{XC}}}{\partial \tilde{\tau}} = \frac{\partial g^{\mathrm{XC}}}{\partial \tau}$. This allows for a straightforward generalization of existing implementations.[20,22,31] The spin-part reads

$$\begin{aligned} X^u_{\mu\nu} = {} & \frac{1}{2}\frac{m_u}{m^s}\int\left[\frac{\partial g^{\mathrm{XC}}}{\partial \rho_\uparrow} - \frac{\partial g^{\mathrm{XC}}}{\partial \rho_\downarrow}\right]\mu\nu\ \mathrm{d}^3r + \frac{1}{2}\frac{m_u}{m^s}\int\left[\frac{|\vec{j}^\uparrow|^2}{2\left(\rho^\uparrow\right)^2}\frac{\partial g^{\mathrm{XC}}}{\partial \tilde{\tau}^\uparrow} - \frac{|\vec{j}^\downarrow|^2}{2\left(\rho^\downarrow\right)^2}\frac{\partial g^{\mathrm{XC}}}{\partial \tilde{\tau}^\downarrow}\right]\mu\ \nu\ \mathrm{d}^3r - \frac{1}{2}\int\left[\frac{\partial g^{\mathrm{XC}}}{\partial \gamma^{\uparrow\uparrow}} + \frac{\partial g^{\mathrm{XC}}}{\partial \gamma^{\downarrow\downarrow}} - \frac{\partial g^{\mathrm{XC}}}{\partial \gamma^{\uparrow\downarrow}}\right]\vec{\nabla}m_u \\ & \cdot\left[\{\vec{\nabla}\mu\}\nu + \mu\{\vec{\nabla}\nu\}\right]\mathrm{d}^3r - \frac{1}{2}\int\left[\frac{\partial g^{\mathrm{XC}}}{\partial \gamma^{\uparrow\uparrow}} - \frac{\partial g^{\mathrm{XC}}}{\partial \gamma^{\downarrow\downarrow}}\right]f_\nabla\frac{\left(\vec{\nabla}\rho^0 \cdot \vec{\nabla}m_u\right)\vec{\nabla}\rho^0}{\Gamma}\ \cdot\left[\{\vec{\nabla}\mu\}\nu + \mu\{\vec{\nabla}\nu\}\right]\mathrm{d}^3r \\ & + \frac{1}{4}\int\left[\frac{\partial g^{\mathrm{XC}}}{\partial \tilde{\tau}^\uparrow} - \frac{\partial g^{\mathrm{XC}}}{\partial \tilde{\tau}^\downarrow}\right]f_\tau\frac{u_u}{|\mathbf{u}|}\left[\vec{\nabla}\mu\right]\cdot\left[\vec{\nabla}\nu\right]\mathrm{d}^3r + \frac{\mathrm{i}}{4}\int\sum_\alpha\left[\frac{j_\alpha^\uparrow}{\rho^\uparrow}\frac{\partial g^{\mathrm{XC}}}{\partial \tilde{\tau}^\uparrow} - \frac{j_\alpha^\downarrow}{\rho^\downarrow}\frac{\partial g^{\mathrm{XC}}}{\partial \tilde{\tau}^\downarrow}\right]f_{j,\alpha}\frac{Y_{\alpha,u}}{|\mathbf{Y}_\alpha|}\left[\{\nabla_\alpha\mu\}\nu - \mu\{\nabla_\alpha\nu\}\right]\mathrm{d}^3r. \end{aligned} \tag{27}$$

That is, a new quadratic or diamagnetic term arises for the density part, and a new linear or paramagnetic term arises for a gradient-like part. Note that functional derivatives are formed with respect to the generalized kinetic energy density, and the expressions are evaluated numerically on a grid.[57–59] The total and spin contributions are then sorted onto the complex two-component Kohn–Sham matrix as described previously.[31] Equations (26) and (27) neglect the derivative of the sign function, which would lead to 2δ, with δ being

the Dirac delta function.[56] Assuming that this contribution is vanishing for nearly all points in space, we deem this to be a suitable approximation.

In the closed-shell limit, the quadratic term in the current density only contributes to the particle contribution $X^0_{\mu\nu}$, whereas the linear term only contributes to the spin contribution $X^u_{\mu\nu}$. The latter can be simplified to

$$\begin{aligned} X^u_{\mu\nu} &= \frac{\mathrm{i}}{4}\int \sum_\alpha \left[\frac{1}{2\rho^\uparrow}\frac{\partial g^{\mathrm{XC}}}{\partial \tilde{\tau}^\uparrow} + \frac{1}{2\rho^\downarrow}\frac{\partial g^{\mathrm{XC}}}{\partial \tilde{\tau}^\downarrow}\right] \\ &\quad \times Y_{\alpha,u}[\{\nabla_\alpha \mu\}\nu - \mu\{\nabla_\alpha \nu\}]\mathrm{d}^3 r \\ &= \frac{\mathrm{i}}{2}\int \sum_\alpha \frac{1}{\rho^0}\frac{\partial g^{\mathrm{XC}}}{\partial \tilde{\tau}} Y_{\alpha,u}[\{\nabla_\alpha \mu\}\nu - \mu\{\nabla_\alpha \nu\}]\mathrm{d}^3 r. \end{aligned} \tag{28}$$

So, all three spin current densities will naturally contribute.

For local hybrid functionals,[60,61] we additionally use the generalized kinetic energy density $\tilde{\tau}$ to construct the local mixing function (LMF) of the Hartree–Fock (HF) exchange. This function may depend on the iso-orbital indicator (t-LMF),[60] the correlation length (z-LMF),[62] or more complicated quantities.[63,64] For instance, the most frequently used t-LMF[60] is then given by

$$a(\vec{r}) = c_t \frac{\tau^{\mathrm{vW}}}{\tilde{\tau}} = c_t \frac{|\vec{\nabla}\rho^0|^2}{8\rho^0 \tilde{\tau}}, \tag{29}$$

where c_t is an empirical parameter and τ^{vW} is the von Weizsäcker kinetic energy density. Note that we only consider common LMFs, which depend on total density variables or the sum of the up and down channels.[65–67] Here, this class of functionals is evaluated with seminumerical integration techniques.[68,69]

We finally consider the numerical stability of the current terms following the ideas of Ref. 53. In regions where the norm of the spin current density $|\vec{Y}_\alpha|$ is close to zero (10^{-16} herein), we suggest using the generalization

$$j^{\uparrow,\downarrow}_\alpha = \frac{1}{2}\left(j^0_\alpha \pm \frac{f_{j,\alpha}}{3}[Y_{\alpha,x} + Y_{\alpha,y} + Y_{\alpha,z}]\right), \tag{30}$$

to avoid the near zero denominator. While ultimately Eq. (30) will break noncollinearity, this price needs to be paid for numerical stability. Furthermore, we also check for collinearity at every point in space. That is, only m_z is used in regions where $\sqrt{m_x^2 + m_y^2}$ is smaller than 5×10^{-12}. The same applies for the other two combinations. For the current density, we consider nine different cases, e.g., only $Y_{\alpha,z}$ is included if $\sqrt{Y^2_{\alpha,x} + Y^2_{\alpha,y}}$ is small. This is important for tight self-consistent field (SCF) convergence behavior in strong magnetic fields. Here, the collinear limit has to be strictly approached in non-relativistic calculations.

In the present work, this ansatz was implemented into TURBOMOLE[70–72] for ground-state energies and densities, geometry gradients, as well as stress tensors. Stress tensors are only available with periodic boundary conditions.[73–76] Interfaces for Libxc are used to ensure support of many functional approximations.[77,78] Here, the functional derivatives such as $(\partial g^{\mathrm{XC}}/\partial \rho_\uparrow)$ or $(\partial g^{\mathrm{XC}}/\partial \tilde{\tau}_\uparrow)$ can be directly evaluated with the existing unrestricted Kohn–Sham routines.

III. COMPUTATIONAL METHODS

First, the closed-shell limit is considered using the At_2 molecule (bond length 293.06 pm, 5.537 973 909 676 10 a_0). Here, relativistic effects are either introduced with modified Dirac–Fock effective core potentials[79] (mDF-ECP60) or all-electron relativistic exact two-component (X2C) theory.[80,81] For the first option, we use the dhf-TZVP-2c basis set,[82] whereas the x2c-QZVPall-2c[83] basis set with a finite nucleus model[84] (Gaussian charge distribution) is employed for X2C. Large grids[85] (grid size 7a), tight SCF thresholds of at least 10^{-10} Hartree and 10^{-9} for the root mean square change of the density matrix (scfconv 10, denconv 1.0×10^{-9}), and a complex generalized direct inversion of the iterative subspace (GDIIS) are applied. The TPSS,[42] TPSSh,[43] r^{2}SCAN,[38,39] TASK,[40] TMHF,[67] CHYF-PBE,[64] LH12ct-SsirPW92[65] (LH12ct), and mPSTS-a1[26,63] functionals are used. The latter four represent the class of LHFs.

Second, the closed-shell limit is studied for the two-dimensional periodic system $MoSe_2$ in the hexagonal (2H) phase.[86] We use the dhf-TZVP-2c basis set[49] and small-core mDF-ECPs[79,87] with the M06-L,[36] r^{2}SCAN,[38,39] TASK,[40] TPSS,[42] Tao–Mo,[41] and PKZB[88] functionals and a k-mesh of 33×33 points. Further computational settings are the same as in Ref. 32, and we refer to this reference for details.

Third, the rotational invariance of the open-shell I_2^+ (bond length 273.82 pm, 5.174 358 200 120 0 a_0) molecule in the presence of SOC is studied. This is performed with the dhf-SVP-2c basis sets[82] and small-core mDF-ECPs.[89] The local density approximation (LDA) S-VWN (V-fit),[90,91] PBE,[92] PBE0,[93] LC-ωPBE,[94] TPSS,[42] TPSSh,[43] M06-L,[36] revM11,[95] and CHYF-PBE[64] DFAs as well as HF are applied. We use the reference grid,[57,58,96,97] scfconv 12, denconv 1.0×10^{-9}, and do not make use of the numerical stabilization for regions with (almost) vanishing spin magnetization or spin current density. Checks for local collinearity are still applied. For comparison, results with more common settings and a standard grid are shown in the Appendix. To check for artifacts due to the high symmetry, the IAt^+ molecule is further considered (bond length 275.88 pm, 5.213 443 584 451 0 a_0) with the same settings.

Fourth, the He_7 molecule in a strong magnetic field of 2 B_0 (≈470 104 T) is studied. Two spin states are considered, namely the S = 0 state with a He–He bond length of 104.4 pm and the S = 7 state with bond lengths of 139.1 pm. Nonrelativistic calculations[18,98,99] are performed with TPSS[42] and TASK[40] (grid size 5, scfconv 10, and denconv 1.0^{-8}) using the decontracted aug-cc-pVTZ basis set[100] and London atomic orbitals for gauge origin invariance. Generally, strong fields require tailored basis sets, and especially the original contraction coefficients of common basis set families are unsuited. Therefore, the decontracted form is used; a detailed analysis of the basis set error in atomic calculations can be found in Ref. 101. Finite field calculations do not make use of the alternative expressions for vanishing spin magnetization and current densities.

IV. RESULTS AND DISCUSSION

A. Rotational invariance for the closed-shell limit with SOC

In the closed-shell limit, the spin magnetization vanishes, but all three spin current densities are generally non-zero. Therefore,

TABLE I. Total energies and energy differences for the At_2 molecule aligned along the Cartesian axes at the mDFT-ECP60/dhf-TZVP-2c level. X2C results are available in the supplementary material. For the x axis, the total SCF energy is listed, whereas the respective energy difference is listed for y and z. All values are given in Hartree. CDFT can and CDF SFT denote the canonical formalism and the Scalmani–Frisch ansatz, respectively. DFT refers to the Kramers-restricted two-component DFT approach.

DFA	Axis	DFT	CDFT can	CDFT SF
TPSS	x	−525.577 087 7	−525.577 516 7	−525.578 315 0
	y	$<1.00 \times 10^{-10}$	$<1.00 \times 10^{-10}$	$<1.00 \times 10^{-10}$
	z	$<1.00 \times 10^{-10}$	6.27×10^{-5}	$<1.00 \times 10^{-10}$
TPSSh	x	−525.585 232 0	−525.585 619 8	−525.586 340 9
	y	$<1.00 \times 10^{-10}$	$<1.00 \times 10^{-10}$	$<1.00 \times 10^{-10}$
	z	$<1.00 \times 10^{-10}$	5.73×10^{-5}	$<1.00 \times 10^{-10}$
r^2SCAN	x	−525.956 154 1	−525.958 053 3	−525.961 791 3
	y	$<1.00 \times 10^{-10}$	$<1.00 \times 10^{-10}$	$<1.00 \times 10^{-10}$
	z	$<1.00 \times 10^{-10}$	6.92×10^{-5}	$<1.00 \times 10^{-10}$
TASK	x	−526.438 617 3	−526.442 464 2	−526.450 094 4
	y	$<1.00 \times 10^{-10}$	$<1.00 \times 10^{-10}$	$<1.00 \times 10^{-10}$
	z	$<1.00 \times 10^{-10}$	6.64×10^{-5}	$<1.00 \times 10^{-10}$
TMHF	x	−525.749 833 1	−525.749 735 5	−525.749 562 9
	y	3.00×10^{-10}	$<1.00 \times 10^{-10}$	$<1.00 \times 10^{-10}$
	z	2.00×10^{-10}	-2.01×10^{-5}	$<1.00 \times 10^{-10}$
CHYF-PBE	x	−525.453 358 2	−525.453 993 9	−525.455 286 8
	y	$<1.00 \times 10^{-10}$	$<1.00 \times 10^{-10}$	$<1.00 \times 10^{-10}$
	z	$<1.00 \times 10^{-10}$	-1.33×10^{-5}	$<1.00 \times 10^{-10}$
LH12ct	x	−525.331 364 9	−525.331 519 6	−525.331 936 6
	y	$<1.00 \times 10^{-10}$	2.49×10^{-8}	7.53×10^{-8}
	z	$<1.00 \times 10^{-10}$	-1.06×10^{-4}	-2.35×10^{-8}
mPSTS-a1	x	−525.587 919 6	−525.588 310 8	−525.589 030 4
	y	$<1.00 \times 10^{-10}$	$<1.00 \times 10^{-10}$	$<1.00 \times 10^{-10}$
	z	$<1.00 \times 10^{-10}$	6.23×10^{-5}	$<1.00 \times 10^{-10}$

the energy with CDFT differs from standard DFT, as shown by the results listed in Table I. In line with previous studies,[26–32] the largest impact is observed for TASK, followed by r^2SCAN. For semilocal functionals, the inclusion of the current density leads to a lower energy. Hybrid functionals show smaller changes, and the energy may also decrease in absolute numbers depending on the functional. Here, Hartree–Fock exchange always includes contributions from the antisymmetric parts of the density matrix naturally (see, for instance, Refs. 49 and 102). In the framework of DFT, these only arise when spin current densities are used. For local hybrids, the interplay between the semilocal DFT parts and the Hartree–Fock exchange through the LMF is the decisive point. Here, the von Weizsäcker inequality does not hold without current densities,[20] and LHFs become formally ill-defined—especially those with the t-LMF and the iso-orbital indicator.

Both DFT and CDFT SF are numerically rotationally invariant for At_2. That is, the same energy is obtained regardless of the aligned axis. For the canonical CDFT approach, the results for the x and y alignments agree, but deviations for the z alignment are observed. Notably, LH12ct already shows rather large deviations between the x and y alignment. This is in line with our previous studies,[26,31,67] where we observed a sub-optimal SCF convergence behavior for the t-LMF with very tight thresholds.

In detail, the canonical CDFT formalism effectively only includes the spin-z current density, as shown by results in the supplementary material. This can be rationalized by the projection of the spin current densities onto the spin magnetization vector. Here, m_z is extremely small, but it is still the largest component, and the term m_u/m^s is numerically challenging. The SF formalism avoids this projection and, therefore, it naturally considers all three spin current densities, which is crucial to restoring rotational invariance. Consequently, the energy change from DFT to CDFT with the SF ansatz is roughly three times as large as with the canonical approach. This is due to the fact that the energy of the At_2 molecule may be roughly approximated by two non-interacting At atoms. Therefore, the approximate spherical symmetry around the At atoms leads to the same result for the derivatives of g in the XC potential. In addition, the current density is divergence free in the non-relativistic limit. Therefore, a factor of approximately three is found.

It is possible to use the definitions of Eqs. (22) and (23) in the closed-shell limit for the canonical formalism to define a so-called modified canonical approach, which would be rotationally invariant. However, the canonical formalism does not naturally lead to this limit for $\tilde{\tau}$ when studying the transition from a closed-shell to an open-shell system, e.g., the transition from a non-magnetic to a magnetic material, cf. Refs. 76 and 103. In this sense, the SF formalism is preferred over such a modified canonical approach.

B. Rashba splittings of $MoSe_2$ in 2H phase

We now study if the SF formalism leads to changes for properties such as bandgaps and Rashba splittings. Here, the two-dimensional dichalcogenide system $MoSe_2$ is one of the archetype systems with a pronounced Rashba splitting.[86,104,105] The results are presented in Table II and confirm the large splitting found in the literature[86,105] with the PBE functional and relativistic all-electron approaches. Previously, it was shown that the generalization of the kinetic energy density may be important for Rashba splittings of such dichalcogenide systems.[32,34,106] Here, Desmarais *et al.* studied the impact of the spin current densities for the r^2SCAN functional and showed that the generalization is crucial.[34,106] However, the impact is comparably small for functionals such as the PZKB or

TABLE II. Bandgaps and Rashba splittings of the valence band at the K point for $MoSe_2$ (hexagonal 2H phase) at the two-component level with the dhf-TZVP-2c basis set and the mDF-ECP10/mDF-ECP28 for Se and Mo, respectively. All values are in eV. The results with DFT and the canonical CDFT approach are taken from Ref. 32.

	Bandgap			Rashba splitting		
DFA	DFT	CDFT can	CDFT SF	DFT	CDFT can	CDFT SF
PKZB	1.455	1.455	1.453	0.166	0.169	0.169
Tao–Mo	1.459	1.458	1.457	0.166	0.170	0.170
TPSS	1.459	1.458	1.455	0.167	0.174	0.174
M06-L	1.460	1.455	1.453	0.170	0.181	0.182
r^2SCAN	1.554	1.544	1.542	0.166	0.189	0.189
TASK	1.629	1.607	1.605	0.172	0.218	0.217

TPSS functionals.[32] Studies on magnetic and electromagnetic properties revealed a similar trend in relativistic and non-relativistic calculations.[27,29,31,107]

In line with previous studies, the CDFT framework leads to notable changes for M06-L, r^{2}SCAN, and TASK, whereas the other DFAs are rather insensitive toward the current density. The canonical and SF formalisms lead to very similar results. For the given precision, the same results are obtained for all DFAs but TASK.

C. Rotational invariance for open-shell SOC calculations

Having established the formalism for closed-shell systems, we now turn to open-shell calculations with SOC. Total energies and energy differences for different orientations of I_2^+ and AtI^+ are listed in Tables III and IV. The results with more standard computational settings (grid, thresholds) are shown in the Appendix and explicitly do not make use of symmetry. Tables III and IV further employ very large reference grids. However, they show that even for the LDA formalism, which is rotationally invariant in each formalism, a slight error remains. Overall, more than ten significant digits of total accuracy cannot be achieved within DFT. This error stems from the construction of the numerical grid, which is not rotationally invariant when no symmetry is used in its construction.[57] This rotational variance in grid construction is enhanced for the more complex GGA, *meta*-GGA, and local hybrid functionals when compared to LDAs, though it never reaches a critical level. Tables III and IV further outline that especially current-dependent *meta*-GGA formulations within the SF are also not much more sensitive than LDAs overall, outlining the correctness of the implementation. Introducing the rotationally invariant SF formulation, consequently, therefore, reliably reduces the error obtained by rotating the molecule to the numerical error in the grid construction also observed for LDA. We further note that all errors are well within the limits of the numerical accuracy obtainable for most functionals, where especially *meta*-GGAs tend to be troublesome.[108] In contrast, wave function based methods that do not rely on numerical integration grids will not suffer from this issue, yielding results that are essentially converged to the numerical precision of the calculation.

D. Application to He_7 in finite magnetic fields

We close our investigation by examining the effects of strong magnetic fields on a helium cluster, comparing the performance of the SF and the canonical formalism in the framework of CDFT. Magnetic fields of the order of magnitude considered here can be found in the atmosphere of interstellar objects such as magnetic white dwarfs.[109–111] Helium is an abundant element in such environments, where it often acts as a thick envelope encasing a core consisting of heavier elements.[112,113] From a physical or chemical perspective, helium is a fascinating species in these extreme conditions, as computational studies have predicted that the noble gas can

TABLE III. Total energies and energy differences for the I_2^+ molecule aligned along the x, y, z axis and the xy, xz, yz diagonal at the mDF-ECP28/dhf-SVP-2c level. The initial guess of the magnetization was chosen along the molecular axis, and energies are given in Hartree. Inclusion of the current density is indicated by a "c" for the functional acronym. S-VWN, PBE, PBE0, and LC-ωPBE are considered for comparison. The can and SF formalism are identical for S-VWN. Functionals for all four first rungs of Jacob's ladder are included.

DFA	Formalism	x axis	y axis	z axis	xy diagonal	xz diagonal	yz diagonal
HF	⋯	−589.048 713 4	$<1.00\times10^{-10}$	$<1.00\times10^{-10}$	$<1.00\times10^{-10}$	$<1.00\times10^{-10}$	$<1.00\times10^{-10}$
S-VWN	can	−590.332 658 0	$<1.00\times10^{-10}$	$<1.00\times10^{-10}$	-7.14×10^{-7}	-7.14×10^{-7}	-7.14×10^{-7}
PBE	SF	−591.133 732 6	$<1.00\times10^{-10}$	$<1.00\times10^{-10}$	-7.93×10^{-7}	-7.93×10^{-7}	-7.93×10^{-7}
PBE0	SF	−591.166 906 4	$<1.00\times10^{-10}$	$<1.00\times10^{-10}$	-6.25×10^{-7}	-6.25×10^{-7}	-6.25×10^{-7}
LC-ωPBE	SF	−591.194 146 4	$<1.00\times10^{-10}$	-4.69×10^{-9}	-8.59×10^{-7}	-8.60×10^{-7}	-8.59×10^{-7}
TPSS	SF	−591.497 899 8	-1.10×10^{-7}	1.10×10^{-7}	-2.11×10^{-6}	-2.11×10^{-6}	-2.11×10^{-6}
cTPSS	SF	−591.499 183 9	2.12×10^{-9}	1.66×10^{-9}	-3.39×10^{-6}	-3.40×10^{-6}	-3.40×10^{-6}
cTPSS	can	−591.498 885 9	$<1.00\times10^{-10}$	$<1.00\times10^{-10}$	-2.26×10^{-6}	-2.26×10^{-6}	-2.26×10^{-6}
TPSSh	SF	−590.930 260 8	$<1.00\times10^{-10}$	$<1.00\times10^{-10}$	-5.17×10^{-7}	-5.17×10^{-7}	-5.17×10^{-7}
cTPSSh	SF	−590.930 773 3	-4.80×10^{-10}	$<1.00\times10^{-10}$	-7.06×10^{-7}	-7.06×10^{-7}	-7.06×10^{-7}
cTPSSh	can	−590.930 649 6	$<1.00\times10^{-10}$	$<1.00\times10^{-10}$	-8.36×10^{-7}	-8.36×10^{-7}	-8.36×10^{-7}
M06-L	SF	−590.964 163 8	$<1.00\times10^{-10}$	$<1.00\times10^{-10}$	-7.19×10^{-7}	-7.19×10^{-7}	-7.19×10^{-7}
cM06-L	SF	−590.964 631 5	$<1.00\times10^{-10}$	$<1.00\times10^{-10}$	-9.74×10^{-7}	-9.74×10^{-7}	-9.74×10^{-7}
cM06-L	can	−590.964 520 1	$<1.00\times10^{-10}$	$<1.00\times10^{-10}$	-9.50×10^{-7}	-9.50×10^{-7}	-9.50×10^{-7}
revM11	SF	−591.005 522 6	-1.62×10^{-8}	-1.84×10^{-8}	-5.91×10^{-7}	-3.82×10^{-7}	-4.70×10^{-7}
crevM11	SF	−591.004 274 0	-8.48×10^{-8}	3.72×10^{-9}	-3.20×10^{-6}	-3.20×10^{-6}	-3.20×10^{-6}
crevM11	can	−591.004 682 3	$<1.00\times10^{-10}$	$<1.00\times10^{-10}$	-1.40×10^{-6}	-1.40×10^{-6}	-1.40×10^{-6}
CHYF-PBE	SF	−590.841 578 5	-4.10×10^{-10}	-4.20×10^{-10}	-1.57×10^{-6}	-1.58×10^{-6}	-1.57×10^{-6}
cCHYF-PBE	SF	−590.842 152 3	$<1.00\times10^{-10}$	$<1.00\times10^{-10}$	-1.19×10^{-6}	-1.19×10^{-6}	-1.19×10^{-6}
cCHYF-PBE	can	−590.842 041 1	$<1.00\times10^{-10}$	2.42×10^{-8}	-1.20×10^{-6}	-1.19×10^{-6}	-1.19×10^{-6}

TABLE IV. Total energies and energy differences for the IAt^+ molecule aligned along the x, y, z axis and the xy, xz, yz diagonal at the mDF-ECP28/dhf-SVP-2c level. See Table III for details.

DFA	Formalism	x axis	y axis	z axis	xy diagonal	xz diagonal	yz diagonal
HF	⋯	−556.103 148 6	$<1.00 \times 10^{-10}$	$<1.00 \times 10^{-10}$	$<1.00 \times 10^{-10}$	-9.41×10^{-8}	-9.41×10^{-8}
S-VWN	can	−557.580 141 6	$<1.00 \times 10^{-10}$	$<1.00 \times 10^{-10}$	-1.02×10^{-6}	-1.02×10^{-6}	-1.02×10^{-6}
PBE	SF	−558.306 934 0	$<1.00 \times 10^{-10}$	$<1.00 \times 10^{-10}$	-1.23×10^{-6}	-1.23×10^{-6}	-1.23×10^{-6}
PBE0	SF	−558.304 475 9	$<1.00 \times 10^{-10}$	$<1.00 \times 10^{-10}$	-9.41×10^{-7}	-9.41×10^{-7}	-9.41×10^{-7}
LC-ωPBE	SF	−558.350 856 1	$<1.00 \times 10^{-10}$	$<1.00 \times 10^{-10}$	-1.32×10^{-6}	-1.32×10^{-6}	-1.32×10^{-6}
TPSS	SF	−558.585 186 7	$<1.00 \times 10^{-10}$	$<1.00 \times 10^{-10}$	-3.75×10^{-6}	-3.75×10^{-6}	-3.75×10^{-6}
cTPSS	SF	−558.587 509 2	$<1.00 \times 10^{-10}$	$<1.00 \times 10^{-10}$	-2.02×10^{-5}	-2.02×10^{-5}	-2.02×10^{-5}
cTPSS	can	−558.586 324 2	$<1.00 \times 10^{-10}$	$<1.00 \times 10^{-10}$	-3.72×10^{-6}	-3.72×10^{-6}	-3.72×10^{-6}
TPSSh	SF	−558.098 660 0	$<1.00 \times 10^{-10}$	$<1.00 \times 10^{-10}$	-1.19×10^{-6}	-1.19×10^{-6}	-1.19×10^{-6}
cTPSSh	SF	−558.099 611 8	-3.90×10^{-10}	$<1.00 \times 10^{-10}$	-3.25×10^{-7}	-3.23×10^{-7}	-3.23×10^{-7}
cTPSSh	can	−558.099 089 6	$<1.00 \times 10^{-10}$	$<1.00 \times 10^{-10}$	-1.22×10^{-6}	-1.22×10^{-6}	-1.22×10^{-6}
M06-L	SF	−558.118 836 2	$<1.00 \times 10^{-10}$	-7.10×10^{-8}	-1.14×10^{-6}	-1.14×10^{-6}	-1.14×10^{-6}
cM06-L	SF	−558.119 699 3	$<1.00 \times 10^{-10}$	$<1.00 \times 10^{-10}$	-5.20×10^{-7}	-5.91×10^{-7}	-5.20×10^{-7}
cM06-L	can	−558.119 227 5	$<1.00 \times 10^{-10}$	$<1.00 \times 10^{-10}$	-1.02×10^{-6}	-1.02×10^{-6}	-1.02×10^{-6}
revM11	SF	−558.174 938 9	$<1.00 \times 10^{-10}$	$<1.00 \times 10^{-10}$	-2.99×10^{-7}	-3.00×10^{-7}	-3.00×10^{-7}
crevM11	SF	−558.171 303 0	-9.30×10^{-10}	1.42×10^{-8}	-7.92×10^{-6}	-7.92×10^{-6}	-7.92×10^{-6}
crevM11	can	−558.173 476 7	$<1.00 \times 10^{-10}$	$<1.00 \times 10^{-10}$	8.22×10^{-7}	8.21×10^{-7}	8.21×10^{-7}
CHYF-PBE	SF	−557.987 481 2	1.18×10^{-8}	1.18×10^{-8}	-2.09×10^{-6}	-2.09×10^{-6}	-2.09×10^{-6}
cCHYF-PBE	SF	−557.988 796 0	$<1.00 \times 10^{-10}$	-3.52×10^{-8}	8.70×10^{-7}	8.69×10^{-7}	8.69×10^{-7}
cCHYF-PBE	can	−557.988 051 7	$<1.00 \times 10^{-10}$	-1.23×10^{-8}	-2.18×10^{-6}	-2.18×10^{-6}	-2.18×10^{-6}

form an exotic type of bond here.[114] This perpendicular paramagnetic bonding mechanism is responsible for a strongly bound helium dimer and the formation of larger helium clusters.[115–118]

Investigations of the molecular and electronic structure in the presence of strong magnetic fields necessitate a finite field approach and the use of London atomic orbitals to ensure gauge origin invariance.[119,120] A spin-noncollinear approach must be employed if the magnetic field is not aligned in a parallel direction to the Cartesian z axis ($\vec{B} \nparallel z$).[121–124] However, it should be emphasized that strong magnetic fields align the spin magnetization vector in an antiparallel direction to the field, automatically leading to spin collinearity. In addition, a magnetic field along the, e.g., z axis only induces a spin-z current density, while the spin-x and spin-y components vanish identically. As a consequence, both the SF and canonical CDFT formalisms should formally yield identical results for closed and open shell cases, regardless of the direction of the external magnetic field.

We now examine the He_7 cluster in a magnetic field of 2 B_0 (≈470 104 T), which is depicted in Fig. 1. The structure was optimized with the external magnetic field (z) aligned in a perpendicular direction to the molecular plane (xy). Both the low-spin state (S = 0) and the high-spin state (S = 7) are considered. The TPSS functional was chosen for this optimization because a previous study has demonstrated that it yields similar results to the exact solution (full configuration interaction) for both the bond length and dissociation energy of the helium dimer in its lowest singlet state.[14,117] Using the obtained structures for the low and high-spin states of He_7, the magnetic field was applied in a parallel direction to the three Cartesian axes. Single point calculations were performed for these

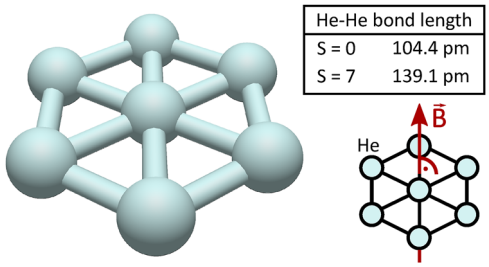

FIG. 1. Molecular structure of He_7 with bond lengths for different spin states (S = 0 and S = 7). The magnetic field B (red color) is perpendicular to the molecular plane.

systems, which are of C_{2h} $\vec{B}\|$ x,y and C_{6h} $\vec{B}\|$ z point group symmetry, respectively.[125] As shown in Table V, the SF and canonical formalisms agree up to the numerical accuracy of the calculations for both the low and high-spin states. All permutations of the molecular plane (xy, xz, yz) and the magnetic field (x, y, z) are considered, demonstrating the expected rotational invariance of the entire system (molecule and magnetic field).

As expected, the SF and canonical formalisms yield identical results for nonrelativistic CDFT calculations in very strong magnetic fields. For relativistic calculations in finite magnetic fields,[126] we consequently expect the two formalisms to also converge toward the same result with increasing field strengths; i.e., in the strong-field limit, the Zeeman effects dominate over spin–orbit coupling.

TABLE V. Total energies in Hartree for different placements of the He_7 molecule and orientations of the magnetic field vector $\vec{B}$ at the CDFT level with the decontracted aug-cc-pVTZ basis set and London atomic orbitals. The magnetic field strength amounts to 2 B_0 (≈470 104 T).

Spin state	DFA	Formalism	Molecular plane	$\vec{B}\parallel$ x axis	$\vec{B}\parallel$ y axis	$\vec{B}\parallel$ z axis
S = 0	TPSS	can	yz plane (x = 0)	−16.472 569 201 18	−16.136 103 393 95	−16.029 770 490 66
			xz plane (y = 0)	−16.029 770 490 66	−16.472 569 201 18	−16.136 103 393 95
			xy plane (z = 0)	−16.136 103 393 95	−16.029 770 490 66	−16.472 569 201 18
S = 0	TPSS	SF	yz plane (x = 0)	−16.472 569 201 15	−16.136 103 393 88	−16.029 770 490 62
			xz plane (y = 0)	−16.029 770 490 62	−16.472 569 201 15	−16.136 103 393 88
			xy plane (z = 0)	−16.136 103 393 88	−16.029 770 490 62	−16.472 569 201 15
S = 7	TASK	can	yz plane (x = 0)	−24.404 914 230 48	−24.244 285 028 31	−24.177 612 890 38
			xz plane (y = 0)	−24.177 612 890 38	−24.404 914 230 48	−24.244 285 028 31
			xy plane (z = 0)	−24.244 285 028 31	−24.177 612 890 38	−24.404 914 230 48
S = 7	TASK	SF	yz plane (x = 0)	−24.404 914 230 48	−24.244 285 028 31	−24.177 612 890 38
			xz plane (y = 0)	−24.177 612 890 38	−24.404 914 230 48	−24.244 285 028 13
			xy plane (z = 0)	−24.244 285 028 31	−24.177 612 890 38	−24.404 914 230 48

For closed-shell systems such as the At_2 molecule considered in Sec. IV A, higher field strengths may eventually lead to a fully rotational invariant canonical formalism. However, an explicit analysis of the two formalisms for relativistic calculations in finite magnetic fields remains the subject of future work.

V. CONCLUSION AND OUTLOOK

The noncollinear approach of Scalmani and Frisch was generalized to the framework of current density functional theory and local hybrid functionals. It was successfully applied to two-component relativistic spin–orbit calculations as well as finite magnetic fields in a nonrelativistic framework. Rotational invariance was demonstrated explicitly, and the proper closed-shell limit is obtained. The SF approach is thus to be preferred for formal reasons in the closed-shell limit. Here, it naturally ensures rotational invariance, unlike the canonical formalism. However, the changes compared to the canonical formalism for properties such as bandgaps and Rashba splittings are rather small. The spin current density is, however, of great importance for Rashba splittings with functionals such as r^{2}SCAN or TASK. Both formalisms satisfy the collinear limit and consequently lead to identical results in strong magnetic fields without relativistic effects.

Based on the findings herein, we do not expect substantial changes for nuclear magnetic resonance properties such as shielding tensors[31,127] and spin–spin coupling tensors[31,128] of closed-shell systems. Likewise, the largest impact of the current density was previously found for electron paramagnetic resonance properties,[31] and we do also not expect major changes when using the SF formalism instead of the canonical one for these properties, as these properties are evaluated with three, two, or four-component calculations where the spin magnetization is aligned along three orthogonal axes.[129–136]

The local torque of the SF formalism is, however, pivotal to studying the spin dynamics in, e.g., real-time time-dependent DFT calculations[137,138] or lattices with a noncollinear antiferromagnetic Néel state.[52] We expect the current-dependent generalization to be useful for relativistic calculations of such systems.

SUPPLEMENTARY MATERIAL

Spreadsheets with all results for At_2, IAt^+, and I_2^+ (csv files).

ACKNOWLEDGMENTS

Y.J.F. gratefully acknowledges support via the Walter–Benjamin Program funded by the Deutsche Forschungsgemeinschaft (DFG, German Research Foundation)—No. 518707327. A.P. gratefully acknowledges support from the Walter Benjamin Program funded by the Deutsche Forschungsgemeinschaft (DFG, German Research Foundation) through No. DFG-529675149. C.H. gratefully acknowledges funding by the Volkswagen Foundation.

AUTHOR DECLARATIONS

Conflict of Interest

The authors have no conflicts to disclose.

Author Contributions

Yannick J. Franzke: Conceptualization (lead); Data curation (equal); Formal analysis (equal); Investigation (equal); Methodology (lead); Software (lead); Validation (equal); Visualization (supporting); Writing – original draft (lead); Writing – review & editing (equal). **Ansgar Pausch**: Conceptualization (equal); Data curation (equal); Formal analysis (equal); Investigation (equal); Methodology (equal); Software (equal); Validation (equal); Visualization (equal); Writing – original draft (equal); Writing – review & editing (equal). **Christof Holzer**: Conceptualization (equal); Data curation (supporting); Formal analysis (equal); Investigation

TABLE VI. Total energies and energy differences for the I_2^+ molecule aligned along the x, y, z axis and the xy, xz, yz diagonal at the mDF-ECP28/dhf-QZVP-2c level. The initial guess of the magnetization was chosen along the molecular axis, and energies are given in Hartree. The inclusion of the current density is indicated by a "c" for the functional acronym. S-VWN, PBE, PBE0, and LC-ωPBE are considered for comparison. The can and SF formalism are identical for S-VWN. Functionals for all four first rungs of Jacob's ladder are included.

DFA	Formalism	x axis	y axis	z axis	xy diagonal	xz diagonal	yz diagonal
S-VWN	can	−590.388 712 8	$<1.00 \times 10^{-10}$	$<1.00 \times 10^{-10}$	-6.81×10^{-7}	-6.82×10^{-7}	-6.82×10^{-7}
PBE	SF	−591.181 577 2	$<1.00 \times 10^{-12}$	$<1.00 \times 10^{-10}$	-8.20×10^{-7}	-8.22×10^{-7}	-8.22×10^{-7}
PBE0	SF	−591.216 345 6	$<1.00 \times 10^{-12}$	$<1.00 \times 10^{-10}$	-6.02×10^{-7}	-6.08×10^{-7}	-6.08×10^{-7}
LC-ωPBE	SF	−591.245 437 8	-8.39×10^{-8}	-8.51×10^{-8}	-9.88×10^{-7}	-9.66×10^{-7}	-7.44×10^{-7}
TPSS	SF	−590.979 341 1	$<1.00 \times 10^{-10}$	$<1.00 \times 10^{-10}$	-1.87×10^{-6}	-1.87×10^{-6}	-1.87×10^{-6}
cTPSS	SF	−590.979 874 7	$<1.00 \times 10^{-10}$	9.89×10^{-12}	-2.28×10^{-6}	-2.28×10^{-6}	-2.28×10^{-6}
cTPSS	can	−590.979 732 2	$<1.00 \times 10^{-10}$	$<1.00 \times 10^{-10}$	-1.21×10^{-6}	-1.21×10^{-6}	-1.21×10^{-6}
TPSSh	SF	−591.013 831 5	$<1.00 \times 10^{-10}$	$<1.00 \times 10^{-10}$	-6.65×10^{-7}	-6.75×10^{-7}	-6.82×10^{-7}
cTPSSh	SF	−591.014 320 1	1.33×10^{-9}	$<1.00 \times 10^{-10}$	-3.35×10^{-7}	-3.39×10^{-7}	-3.46×10^{-7}
cTPSSh	can	−591.014 189 7	$<1.00 \times 10^{-10}$	$<1.00 \times 10^{-10}$	-1.06×10^{-6}	-1.06×10^{-6}	-1.06×10^{-6}
M06-L	SF	−591.553 334 1	$<1.00 \times 10^{-10}$	-1.61×10^{-8}	-2.64×10^{-6}	-2.64×10^{-6}	-2.64×10^{-6}
cM06-L	SF	−591.554 771 6	5.50×10^{-10}	7.10×10^{-10}	-3.89×10^{-6}	-3.90×10^{-6}	-3.91×10^{-6}
cM06-L	can	−591.554 359 9	$<1.00 \times 10^{-10}$	$<1.00 \times 10^{-10}$	-2.91×10^{-6}	-2.92×10^{-6}	-2.92×10^{-6}
revM11	SF	−591.061 837 9	-3.15×10^{-8}	1.15×10^{-8}	-4.69×10^{-7}	-5.54×10^{-7}	-4.96×10^{-7}
crevM11	SF	−591.060 225 6	-3.12×10^{-8}	9.55×10^{-9}	-2.21×10^{-6}	-1.99×10^{-6}	-1.99×10^{-6}
crevM11	can	−591.060 856 4	$<1.00 \times 10^{-10}$	3.60×10^{-10}	1.61×10^{-6}	1.93×10^{-6}	1.93×10^{-6}
CHYF-PBE	SF	−590.892 634 7	2.09×10^{-9}	2.82×10^{-8}	-1.19×10^{-6}	-1.20×10^{-6}	-1.20×10^{-6}
cCHYF-PBE	SF	−590.893 348 9	2.33×10^{-9}	2.18×10^{-9}	-1.10×10^{-6}	-1.13×10^{-6}	-1.16×10^{-6}
cCHYF-PBE	can	−590.893 165 2	2.30×10^{-10}	3.58×10^{-8}	-1.08×10^{-6}	-1.07×10^{-6}	-1.07×10^{-6}

(equal); Methodology (equal); Software (equal); Validation (equal); Visualization (supporting); Writing – original draft (supporting); Writing – review & editing (supporting).

DATA AVAILABILITY

The data that support the findings of this study are available within the article and its supplementary material.

APPENDIX: ROTATIONAL INVARIANCE FOR I_2^+ WITH A STANDARD GRID

The rotational invariances of IAt^+ and I_2^+ are also studied with more common settings, and the S-VWN (V-fit),[90,91] PBE,[92] PBE0,[93] LC-ωPBE,[94] TPSS,[42] TPSSh,[43] M06-L,[36] revM11,[95] and CHYF-PBE[64] DFAs as well as HF are applied (grid size 7a, scf-conv 9, and denconv 1.0×10^{-8}, dhf-QZVPall-2c basis set). Table VI shows the energies for different spatial positions or alignments of the I_2^+ molecules. Note that we use one of TURBOMOLE's standard grids[57,58,85] without special settings to allow for a comparison to routine calculations. This ensures rotational invariance up to at least 3×10^{-6} Hartree for all functionals. We note in passing that many *meta*-GGAs are numerically challenging,[108,139,140] and GGAs generally lead to a better agreement of the energies.

Both the canonical and the SF ansatz are invariant for cTPSS and cTPSSh. Energy differences between the two formalisms are due to a slightly larger spin expectation value with the SF formalism and the avoided projection of the spin current densities onto the magnetization vector. We note in passing that the canonical and the SF ansatz lead to the same result when the initial magnetization is kept fixed (no SOC) and the standard DFT framework is applied. With SOC, the SF formalism leads to a lower energy for all DFAs except for revM11, as shown in Table VI.

REFERENCES

[1] M. Brack, B. Jennings, and Y. Chu, Phys. Lett. B **65**, 1 (1976).
[2] A. D. Becke, J. Chem. Phys. **117**, 6935 (2002).
[3] J. Tao, Phys. Rev. B **71**, 205107 (2005).
[4] G. Vignale and M. Rasolt, Phys. Rev. B **37**, 10685 (1988).
[5] G. Vignale and M. Rasolt, Phys. Rev. B **39**, 5475 (1989).
[6] A. Laestadius, Int. J. Quantum Chem. **114**, 1445 (2014).
[7] A. Laestadius and M. Benedicks, Int. J. Quantum Chem. **114**, 782 (2014).
[8] A. Laestadius, J. Math. Chem. **52**, 2581 (2014).
[9] A. Laestadius and M. Benedicks, Phys. Rev. A **91**, 032508 (2015).
[10] E. I. Tellgren, S. Kvaal, E. Sagvolden, U. Ekström, A. M. Teale, and T. Helgaker, Phys. Rev. A **86**, 062506 (2012).
[11] E. I. Tellgren, A. M. Teale, J. W. Furness, K. K. Lange, U. Ekström, and T. Helgaker, J. Chem. Phys. **140**, 034101 (2014).
[12] E. I. Tellgren, S. Kvaal, and T. Helgaker, Phys. Rev. A **89**, 012515 (2014).
[13] E. H. Lieb and R. Schrader, Phys. Rev. A **88**, 032516 (2013).
[14] J. W. Furness, J. Verbeke, E. I. Tellgren, S. Stopkowicz, U. Ekström, T. Helgaker, and A. M. Teale, J. Chem. Theory Comput. **11**, 4169 (2015).
[15] T. J. P. Irons, L. Spence, G. David, B. T. Speake, T. Helgaker, and A. M. Teale, J. Phys. Chem. A **124**, 1321 (2020).
[16] S. Sen and E. I. Tellgren, J. Chem. Theory Comput. **17**, 1480 (2021).
[17] T. J. P. Irons, G. David, and A. M. Teale, J. Chem. Theory Comput. **17**, 2166 (2021).

[18] A. Pausch and C. Holzer, J. Phys. Chem. Lett. **13**, 4335 (2022).
[19] A. M. Lee, N. C. Handy, and S. M. Colwell, J. Chem. Phys. **103**, 10095 (1995).
[20] J. E. Bates and F. Furche, J. Chem. Phys. **137**, 164105 (2012).
[21] S. Reimann, U. Ekström, S. Stopkowicz, A. M. Teale, A. Borgoo, and T. Helgaker, Phys. Chem. Chem. Phys. **17**, 18834 (2015).
[22] J. Liang, X. Feng, D. Hait, and M. Head-Gordon, J. Chem. Theory Comput. **18**, 3460 (2022).
[23] R. Grotjahn and F. Furche, J. Chem. Theory Comput. **19**, 4897 (2023).
[24] C. J. Schattenberg and M. Kaupp, J. Chem. Theory Comput. **17**, 1469 (2021).
[25] Y. J. Franzke, J. Chem. Theory Comput. **19**, 2010 (2023).
[26] C. Holzer, Y. J. Franzke, and M. Kehry, J. Chem. Theory Comput. **17**, 2928 (2021).
[27] Y. J. Franzke and C. Holzer, J. Chem. Phys. **157**, 031102 (2022).
[28] F. Bruder, Y. J. Franzke, and F. Weigend, J. Phys. Chem. A **126**, 5050 (2022).
[29] F. Bruder, Y. J. Franzke, C. Holzer, and F. Weigend, J. Chem. Phys. **159**, 194117 (2023).
[30] Y. J. Franzke, F. Bruder, S. Gillhuber, C. Holzer, and F. Weigend, J. Phys. Chem. A **128**, 670 (2024).
[31] C. Holzer, Y. J. Franzke, and A. Pausch, J. Chem. Phys. **157**, 204102 (2022).
[32] Y. J. Franzke and C. Holzer, J. Chem. Phys. **160**, 184101 (2024).
[33] T. M. Maier, Y. Ikabata, and H. Nakai, J. Chem. Phys. **151**, 174114 (2019).
[34] J. K. Desmarais, J. Maul, B. Civalleri, A. Erba, G. Vignale, and S. Pittalis, Phys. Rev. Lett. **132**, 256401 (2024).
[35] J. K. Desmarais, G. Vignale, K. Bencheikh, A. Erba, and S. Pittalis, Phys. Rev. Lett. **133**, 136401 (2024).
[36] Y. Zhao and D. G. Truhlar, J. Chem. Phys. **125**, 194101 (2006).
[37] Y. Zhao and D. G. Truhlar, Theor. Chem. Acc. **120**, 215 (2008).
[38] J. W. Furness, A. D. Kaplan, J. Ning, J. P. Perdew, and J. Sun, J. Phys. Chem. Lett. **11**, 8208 (2020).
[39] J. W. Furness, A. D. Kaplan, J. Ning, J. P. Perdew, and J. Sun, J. Phys. Chem. Lett. **11**, 9248 (2020).
[40] T. Aschebrock and S. Kümmel, Phys. Rev. Res. **1**, 033082 (2019).
[41] J. Tao and Y. Mo, Phys. Rev. Lett. **117**, 073001 (2016).
[42] J. Tao, J. P. Perdew, V. N. Staroverov, and G. E. Scuseria, Phys. Rev. Lett. **91**, 146401 (2003).
[43] V. N. Staroverov, G. E. Scuseria, J. Tao, and J. P. Perdew, J. Chem. Phys. **119**, 12129 (2003).
[44] J. Kübler, K.-H. Höck, J. Sticht, and A. R. Williams, J. Phys. F Metal Phys. **18**, 469 (1988).
[45] C. Van Wüllen, J. Comput. Chem. **23**, 779 (2002).
[46] T. Saue and T. Helgaker, J. Comput. Chem. **23**, 814 (2002).
[47] J. E. Peralta, G. E. Scuseria, and M. J. Frisch, Phys. Rev. B **75**, 125119 (2007).
[48] M. K. Armbruster, F. Weigend, C. van Wüllen, and W. Klopper, Phys. Chem. Chem. Phys. **10**, 1748 (2008).
[49] A. Baldes and F. Weigend, Mol. Phys. **111**, 2617 (2013).
[50] J. K. Desmarais, S. Komorovsky, J.-P. Flament, and A. Erba, J. Chem. Phys. **154**, 204110 (2021).
[51] G. Scalmani and M. J. Frisch, J. Chem. Theory Comput. **8**, 2193 (2012).
[52] I. W. Bulik, G. Scalmani, M. J. Frisch, and G. E. Scuseria, Phys. Rev. B **87**, 035117 (2013).
[53] F. Egidi, S. Sun, J. J. Goings, G. Scalmani, M. J. Frisch, and X. Li, J. Chem. Theory Comput. **13**, 2591 (2017).
[54] Z. Pu, H. Li, N. Zhang, H. Jiang, Y. Gao, Y. Xiao, Q. Sun, Y. Zhang, and S. Shao, Phys. Rev. Res. **5**, 013036 (2023).
[55] K. Capelle, G. Vignale, and B. L. Györffy, Phys. Rev. Lett. **87**, 206403 (2001).
[56] S. Komorovsky, P. J. Cherry, and M. Repisky, J. Chem. Phys. **151**, 184111 (2019).
[57] O. Treutler and R. Ahlrichs, J. Chem. Phys. **102**, 346 (1995).
[58] O. Treutler, "Entwicklung und Anwendung von Dichtefunktionalmethoden," Ph.D. thesis (Dr. rer. nat.), University of Karlsruhe (TH), Germany, 1995.
[59] A. M. Burow and M. Sierka, J. Chem. Theory Comput. **7**, 3097 (2011).
[60] J. Jaramillo, G. E. Scuseria, and M. Ernzerhof, J. Chem. Phys. **118**, 1068 (2003).
[61] T. M. Maier, A. V. Arbuznikov, and M. Kaupp, Wiley Interdiscip. Rev.: Comput. Mol. Sci. **9**, e1378 (2019).
[62] E. R. Johnson, J. Chem. Phys. **141**, 124120 (2014).
[63] J. P. Perdew, V. N. Staroverov, J. Tao, and G. E. Scuseria, Phys. Rev. A **78**, 052513 (2008).
[64] C. Holzer and Y. J. Franzke, J. Chem. Theory Comput. **21**, 202 (2025).
[65] A. V. Arbuznikov and M. Kaupp, J. Chem. Phys. **136**, 014111 (2012).
[66] A. Wodyński and M. Kaupp, J. Chem. Theory Comput. **16**, 314 (2020).
[67] Y. J. Franzke and C. Holzer, J. Chem. Phys. **157**, 034108 (2022).
[68] P. Plessow and F. Weigend, J. Comput. Chem. **33**, 810 (2012).
[69] C. Holzer, J. Chem. Phys. **153**, 184115 (2020).
[70] R. Ahlrichs, M. Bär, M. Häser, H. Horn, and C. Kölmel, Chem. Phys. Lett. **162**, 165 (1989).
[71] S. G. Balasubramani, G. P. Chen, S. Coriani, M. Diedenhofen, M. S. Frank, Y. J. Franzke, F. Furche, R. Grotjahn, M. E. Harding, C. Hättig, A. Hellweg, B. Helmich-Paris, C. Holzer, U. Huniar, M. Kaupp, A. Marefat Khah, S. Karbalaei Khani, T. Müller, F. Mack, B. D. Nguyen, S. M. Parker, E. Perlt, D. Rappoport, K. Reiter, S. Roy, M. Rückert, G. Schmitz, M. Sierka, E. Tapavicza, D. P. Tew, C. van Wüllen, V. K. Voora, F. Weigend, A. Wodyński, and J. M. Yu, J. Chem. Phys. **152**, 184107 (2020).
[72] Y. J. Franzke, C. Holzer, J. H. Andersen, T. Begušić, F. Bruder, S. Coriani, F. Della Sala, E. Fabiano, D. A. Fedotov, S. Fürst, S. Gillhuber, R. Grotjahn, M. Kaupp, M. Kehry, M. Krstić, F. Mack, S. Majumdar, B. D. Nguyen, S. M. Parker, F. Pauly, A. Pausch, E. Perlt, G. S. Phun, A. Rajabi, D. Rappoport, B. Samal, T. Schrader, M. Sharma, E. Tapavicza, R. S. Treß, V. Voora, A. Wodyński, J. M. Yu, B. Zerulla, F. Furche, C. Hättig, M. Sierka, D. P. Tew, and F. Weigend, J. Chem. Theory Comput. **19**, 6859 (2023).
[73] R. Łazarski, A. M. Burow, and M. Sierka, J. Chem. Theory Comput. **11**, 3029 (2015).
[74] R. Łazarski, A. M. Burow, L. Grajciar, and M. Sierka, J. Comput. Chem. **37**, 2518 (2016).
[75] M. Becker and M. Sierka, J. Comput. Chem. **40**, 2563 (2019).
[76] Y. J. Franzke, W. M. Schosser, and F. Pauly, Phys. Rev. B **109**, 165144 (2024).
[77] "Libxc," Versions 6.2.2 and 7.0.0 (2024), available from https://gitlab.com/libxc/libxc (retrieved October 25, 2024).
[78] S. Lehtola, C. Steigemann, M. J. T. Oliveira, and M. A. L. Marques, SoftwareX **7**, 1 (2018).
[79] K. A. Peterson, D. Figgen, E. Goll, H. Stoll, and M. Dolg, J. Chem. Phys. **119**, 11113 (2003).
[80] D. Peng, N. Middendorf, F. Weigend, and M. Reiher, J. Chem. Phys. **138**, 184105 (2013).
[81] Y. J. Franzke, N. Middendorf, and F. Weigend, J. Chem. Phys. **148**, 104410 (2018).
[82] F. Weigend and A. Baldes, J. Chem. Phys. **133**, 174102 (2010).
[83] Y. J. Franzke, L. Spiske, P. Pollak, and F. Weigend, J. Chem. Theory Comput. **16**, 5658 (2020).
[84] L. Visscher and K. G. Dyall, At. Data Nucl. Data Tables **67**, 207 (1997).
[85] Y. J. Franzke, R. Treß, T. M. Pazdera, and F. Weigend, Phys. Chem. Chem. Phys. **21**, 16658 (2019).
[86] P. Miró, M. Audiffred, and T. Heine, Chem. Soc. Rev. **43**, 6537 (2014).
[87] K. A. Peterson, D. Figgen, M. Dolg, and H. Stoll, J. Chem. Phys. **126**, 124101 (2007).
[88] J. P. Perdew, S. Kurth, A. c. v. Zupan, and P. Blaha, Phys. Rev. Lett. **82**, 2544 (1999).
[89] K. A. Peterson, B. C. Shepler, D. Figgen, and H. Stoll, J. Phys. Chem. A **110**, 13877 (2006).
[90] J. C. Slater, Phys. Rev. **81**, 385 (1951).
[91] S. H. Vosko, L. Wilk, and M. Nusair, Can. J. Phys. **58**, 1200 (1980).
[92] J. P. Perdew, K. Burke, and M. Ernzerhof, Phys. Rev. Lett. **77**, 3865 (1996).
[93] C. Adamo and V. Barone, J. Chem. Phys. **110**, 6158 (1999).
[94] O. A. Vydrov and G. E. Scuseria, J. Chem. Phys. **125**, 234109 (2006).
[95] P. Verma, Y. Wang, S. Ghosh, X. He, and D. G. Truhlar, J. Phys. Chem. A **123**, 2966 (2019).
[96] TURBOMOLE GmbH, developers' version of TURBOMOLE V7.9, a development of University of Karlsruhe and Forschungszentrum Karlsruhe

GmbH, 1989-2007, TURBOMOLE GmbH, since 2007, 2025; available from https://www.turbomole.org (retrieved Janaury 11, 2025).
[97]TURBOMOLE GmbH, manual of TURBOMOLE V7.9, a development of University of Karlsruhe and Forschungszentrum Karlsruhe GmbH, 1989-2007, TURBOMOLE GmbH, since 2007, 2025; available from https://www.turbomole.org/turbomole/turbomole-documentation/ (retrieved January 11, 2025).
[98]A. Pausch and W. Klopper, Mol. Phys. **118**, e1736675 (2020).
[99]L. Monzel, A. Pausch, L. D. M. Peters, E. I. Tellgren, T. Helgaker, and W. Klopper, J. Chem. Phys. **157**, 054106 (2022).
[100]D. E. Woon and T. H. Dunning, J. Chem. Phys. **100**, 2975 (1994).
[101]H. Åström and S. Lehtola, J. Phys. Chem. A **127**, 10872 (2023).
[102]J. K. Desmarais, J.-P. Flament, and A. Erba, Phys. Rev. B **101**, 235142 (2020).
[103]A. Smogunov, A. Dal Corso, A. Delin, R. Weht, and E. Tosatti, Nat. Nanotechnol. **3**, 22 (2008).
[104]Z. Y. Zhu, Y. C. Cheng, and U. Schwingenschlögl, Phys. Rev. B **84**, 153402 (2011).
[105]M. Kadek, B. Wang, M. Joosten, W.-C. Chiu, F. Mairesse, M. Repisky, K. Ruud, and A. Bansil, Phys. Rev. Mater. **7**, 064001 (2023).
[106]A. Boccuni, B. M. T. C. Peluzo, F. Bodo, G. Ambrogio, J. Maul, D. Mitoli, G. Vignale, S. Pittalis, E. Kraka, J. K. Desmarais, and A. Erba, J. Phys. Chem. Lett. **15**, 7442 (2024).
[107]R. Grotjahn, F. Furche, and M. Kaupp, J. Chem. Phys. **157**, 111102 (2022).
[108]S. Lehtola and M. A. L. Marques, J. Chem. Phys. **157**, 174114 (2022).
[109]R. H. Garstang, Rep. Prog. Phys. **40**, 105 (1977).
[110]J. R. P. Angel, Astrophys. J. **216**, 1 (1977).
[111]M. A. Hollands, S. Stopkowicz, M.-P. Kitsaras, F. Hampe, S. Blaschke, and J. J. Hermes, Mon. Not. R. Astron. Soc. **520**, 3560 (2023).
[112]S. Blouin, P. Dufour, C. Thibeault, and N. F. Allard, Astrophys. J. **878**, 63 (2019).
[113]D. Saumon, S. Blouin, and P.-E. Tremblay, Phys. Rep. **988**, 1 (2022).
[114]K. K. Lange, E. I. Tellgren, M. Hoffmann, and T. Helgaker, Science **337**, 327 (2012).
[115]J. Austad, A. Borgoo, E. I. Tellgren, and T. Helgaker, Phys. Chem. Chem. Phys. **22**, 23502 (2020).
[116]M. J. Pemberton, T. J. P. Irons, T. Helgaker, and A. M. Teale, J. Chem. Phys. **156**, 204113 (2022).
[117]A. Pausch, "Development and application of efficient computational methods for molecular spectroscopy in finite magnetic fields," Ph.D. thesis (Dr. rer. nat.), Karlsruhe Institute of Technology, Germany, 2022.
[118]S. Blaschke, S. Stopkowicz, and A. Pausch, J. Chem. Phys. **161**, 024117 (2024).
[119]E. I. Tellgren, A. Soncini, and T. Helgaker, J. Chem. Phys. **129**, 154114 (2008).
[120]M.-P. Kitsaras, L. Grazioli, and S. Stopkowicz, J. Chem. Phys. **160**, 094112 (2024).
[121]S. Sen and E. I. Tellgren, J. Chem. Phys. **148**, 184112 (2018).
[122]S. Sun, D. B. Williams-Young, T. F. Stetina, and X. Li, J. Chem. Theory Comput. **15**, 348 (2019).
[123]C. Holzer, A. Pausch, and W. Klopper, Front. Chem. **9**, 746162 (2021).
[124]A. Pausch, C. Holzer, and W. Klopper, J. Chem. Theory Comput. **18**, 3747 (2022).
[125]A. Pausch, M. Gebele, and W. Klopper, J. Chem. Phys. **155**, 201101 (2021).
[126]S. Sun and X. Li, J. Chem. Theory Comput. **16**, 4533 (2020).
[127]Y. J. Franzke and C. Holzer, J. Chem. Phys. **159**, 184102 (2023).
[128]Y. J. Franzke, F. Mack, and F. Weigend, J. Chem. Theory Comput. **17**, 3974 (2021).
[129]P. Verma and J. Autschbach, J. Chem. Theory Comput. **9**, 1932 (2013).
[130]P. Verma and J. Autschbach, J. Chem. Theory Comput. **9**, 1052 (2013).
[131]I. Malkin, O. L. Malkina, V. G. Malkin, and M. Kaupp, J. Chem. Phys. **123**, 244103 (2005).
[132]M. Repiský, S. Komorovský, E. Malkin, O. L. Malkina, and V. G. Malkin, Chem. Phys. Lett. **488**, 94 (2010).
[133]S. Gohr, P. Hrobárik, M. Repiský, S. Komorovský, K. Ruud, and M. Kaupp, J. Phys. Chem. A **119**, 12892 (2015).
[134]Y. J. Franzke and J. M. Yu, J. Chem. Theory Comput. **18**, 323 (2022).
[135]Y. J. Franzke and J. M. Yu, J. Chem. Theory Comput. **18**, 2246 (2022).
[136]S. Komorovsky, "Relativistic theory of EPR and (p)NMR," in *Comprehensive Computational Chemistry*, 1st ed., edited by M. Yáñez and R. J. Boyd (Elsevier, Oxford, United Kingdom, 2024), pp. 280–314.
[137]J. J. Goings, J. M. Kasper, F. Egidi, S. Sun, and X. Li, J. Chem. Phys. **145**, 104107 (2016).
[138]X. Li, N. Govind, C. Isborn, A. E. I. DePrince, and K. Lopata, Chem. Rev. **120**, 9951 (2020).
[139]S. Lehtola, J. Phys. Chem. A **127**, 4180 (2023).
[140]S. Lehtola, J. Chem. Theory Comput. **19**, 2502 (2023).